Antiquark nuggets as dark matter: New constraints and detection prospects

Peter W. Gorham

Phys. Rev. D **86**, 123005 — Published 7 December 2012

DOI: 10.1103/PhysRevD.86.123005

Antiquark nuggets as dark matter: New constraints and detection prospects

Peter W. Gorham[1]

[1]*Dept. of Physics & Astronomy, Univ. of Hawaii, Manoa, HI 96822.*

Current evidence for dark matter in the universe does not exclude heavy composite nuclear-density objects consisting of bound quarks or antiquarks over a significant range of masses. Here we analyze one such proposed scenario, which hypothesizes antiquark nuggets with a range of $B \sim 10^{24-30}$ with specific predictions for spectral emissivity via interactions with normal matter. We find that, if these objects make up the majority of the dark matter density in the solar neighborhood, their radiation efficiency in solids is marginally constrained, due to limits from the total geothermal energy budget of the Earth. At allowed radiation efficiencies, the number density of such objects can be constrained to be well below dark matter densities by existing radio data over a mass range currently not restricted by other methods.

I. INTRODUCTION

Many different forms of astrophysical and cosmological evidence point to the existence of weakly interacting matter in an unknown form in the universe (see [1] for a recent review), with a total mass of order 30% of the critical density of the universe, and about five times the inventory of what is observed as normal matter in the form of gas, stars, and dust. This gives a *dark matter* density estimated to be in the range $0.4-1$ GeV cm^{-3} in the solar neighborhood [2–4] In addition, current best models for light element production the early universe constrain the fraction of interacting baryons to no more than about 4% of the critical density at the time of nucleosynthesis [1]. Thus candidates for baryonic dark matter are currently disfavored.

These rather compelling arguments for non-baryonic dark matter have led to a wide variety of efforts, both theoretical and experimental, to either postulate or directly detect new particles, beyond the standard model, that would satisfy the dark matter characteristics. However, there remain several "standard-model" candidates for dark matter, which, if not currently favored, have not yet been excluded over all the possible range of parameters. In particular, very massive objects (at least compared to the $\lesssim$TeV scale of typical particle candidates for dark matter) can still satisfy the astrophysical constraints on dark matter if their masses are sufficient that the flux in typical detectors is extremely low, but not so large that they are excluded due to galaxy dynamics or gravitational lensing observations. This may be translated into a constraint on their interaction cross sections per unit mass; current limits require $\sigma/M \lesssim 0.1$ cm^2 g^{-1} [5, 6], a constraint that is in general easily satisfied by neutral objects with nuclear densities.

Such objects must not interact with normal matter via strong or electromagnetic channels at the time of nucleosynthesis. One candidate is the so-called quark nugget, or strangelet, hypothesized originally by Witten [7, 8], and developed in many variations since then. Quark nuggets can be neutral and metastable at their formation during the quantum chromodynamics phase transition of early-universe evolution, and thus do not undergo significant further interactions at nucleosynthesis, therefore evading the constraints on baryonic content.

Although still a matter for debate, the possibility of quark nugget *color superconductivity* [9], in which quarks near the Fermi surface of the nugget form correlated Cooper pairs, favors their possible stability [10]. One of the more attractive aspects of these objects as candidates for dark matter is that the physics of their formation and interactions is in principle calculable according to the standard model, although such calculations can in practice be prohibitively difficult.

Current experimental and observational constraints from seismic energy deposition in the Earth and Moon indicate that quark nuggets can only satisfy dark matter density for baryon numbers $B \lesssim 7 \times 10^{28}$ [14] or $B > 10^{33}$ (but see the possible detection of an event in ref. [13], and the response in [16]). Limits from non-detection of compatible events in the Lake Baikal detector [24] require $B \gtrsim 1.2 \times 10^{20}$.

Considerations of the sensitivity of helium production to the quark nugget surface area at nucleosynthesis [17] lead to a constraint of $B > 10^{22}\ \Omega_{QN} f_n^3$, where Ω_{QN} is the fraction of critical density of the quark nuggets, and $f_n \leq 1$ is the penetrability of the nugget surface. Important limits on quark nuggets in the mass range from micrograms to several grams obtain from searches for etching of tracks on samples of mica [15], and as we discuss in a later section, significant limits in a similar range are given by searches for optical meteor-like events in the terrestrial atmosphere [31, 32].

Very large quark matter objects of several thousand tons or more remain viable dark matter candidates from the point of view of both nucleosynthesis [18] and seismic [14] constraints, but are constrained to a dark matter fraction $<$ 1 by microlensing observations above $B \sim 10^{50}$ or $M \sim 10^{26}$ g. This still leaves a very large range of masses possible, with a window of masses in the several gram to several ton range, and another very large window from million-ton objects up to Earth-mass scales and possibly above. Despite this, it appears that lingering questions about the absolute stability of primordial quark nuggets against evaporation continue to limit their popularity as a dark matter candidate.

In this work we focus on the mass window $10^{20} \leq B \leq 10^{28}$, masses of milligrams to several tons. In this range, fluxes of quark nuggets that could comprise a substantial fraction of the dark matter are accessible to direct detection in terrestrial detectors. Although the lower end of this range is largely excluded, there remains a window several orders of magnitude wide in the mass spectrum in which there are no significant constraints.

II. ANTIQUARK NUGGETS

A recent novel application of the quark nugget hypothesis [19–21, 23] postulates that both antiquark and quark nuggets are formed in the early universe with a ratio of 3:2, and the current observed baryon matter-antimatter asymmetry arises only because the antibaryons are hidden in the excess of antiquark nuggets (AQN), which, along with the quark nuggets form the bulk of the dark matter. AQN have the same kinetic energy as normal quark nuggets, and the transfer of this energy may be observed in seismic [12] or thermal events produced in the Earth's crust. However, in addition to kinetic energy transfer, AQN sweep up and annihilate with normal matter along their track, leading to potentially much more energetic signatures and much higher rates of radiative energy deposition.

Taking an approximate geometric mean value of these constraints, a baryon number of $B \gtrsim 10^{24}$ (~ 1.6 gm) gives a flux of AQN at Earth, assuming they are virialized with Galactic velocities of order 200 km s^{-1}, of order several per km^2 per year if all AQNs were close to this mass; actual fluxes will depend of course on the assumed mass spectrum in the solar neighborhood.

A. AQN thermal emission

It is instructive to consider the flux of AQN at this mass scale to determine the rate of energy deposited in the Earth. Recent detailed calculations of the emissivity of AQN when accreting normal matter have been carried out Thomas-Fermi model to determine the electrosphere structure of the positrons surrounding the AQN, and then estimating its emissivity as a Boltzmann gas of positrons [19, 20] . In this case the spectral emissivity of a nugget at effective temperature T for photon energies well below the electron mass m_e is given by:

$$\frac{dF}{d\omega} \sim \frac{4}{45}\frac{\sigma_{SB}T^3\alpha^{5/2}}{\pi}\left(\frac{T}{m_e}\right)^{\frac{1}{4}} K\left(\frac{\omega}{T}\right) \qquad (1)$$

where σ_{SB} is the Stefan-Boltzmann constant, α is the fine-structure constant, and ω is the angular frequency of the radiation, and

$$K\left(\frac{\omega}{T}\right) = \left(1+\frac{\omega}{T}\right)\left(17-12\log\left[\frac{\omega}{2T}\right]\right)\, e^{-\omega/T}\ .$$

(Here ratios such as ω/T are given with implicit values of Planck's and Boltzmann's constants h, k where necessary to rationalize the units.) This result, converted to spectral power $dP/d\omega = 4\pi R_n^2 dF/d\omega$, is plotted in Fig. 1 for the case of an AQN of $B = 10^{24}$, and a nugget radius estimated [19, 20] to be $R_n = 10^{-7}$ m, for three different AQN surface temperatures.

The integral emissivity over all frequencies, determined from this spectral emissivity is

$$F_{tot} = \frac{d^2E}{dtdA} = \frac{16}{3}\frac{\sigma_{SB}T^4\alpha^{5/2}}{\pi}\left[\frac{T}{m_e}\right]^{\frac{1}{4}} \qquad (2)$$

and is typically a fraction of order 10^{-6} of blackbody emission [19, 21]. Similar levels of suppression of low-frequency emission relative to blackbody levels are estimated for quark matter, for example from the surface of hypothetical strange stars [22], where the suppression can be seen as a plasma-frequency effect. The main difference between quark and antiquark nuggets in this respect is the potentially much higher surface temperature that can obtain due to annihilation of accreted matter. For AQN, the emitted power is also distributed with a spectral emissivity very different from a blackbody, since it is nearly flat at low frequencies as equation 1 and Fig. 1 show.

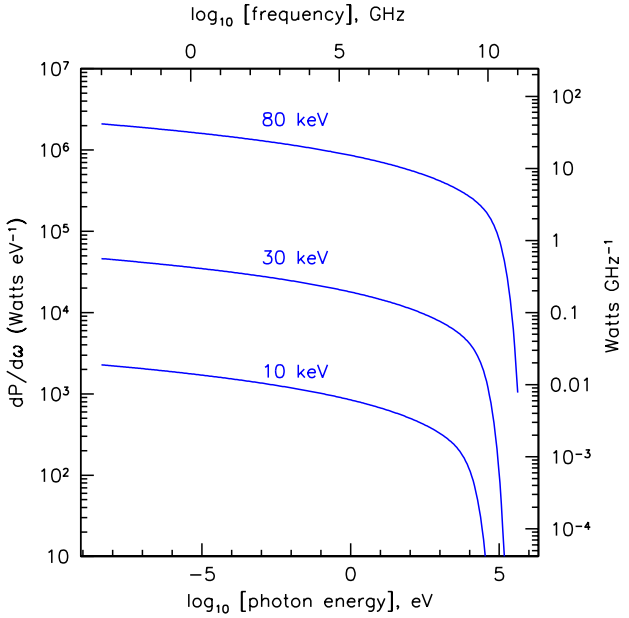

FIG. 1: *Spectral density of emission from a $B \sim 10^{24}$ antiquark nugget for three values of the effective surface temperature.*

B. Temperature upper bound

The temperature of the AQN in equation 1 is determined from the amount of matter accreted and annihilated along the nugget's path, by normalizing the total emission (the integral of this equation over all ω) to equal the fraction $1-g$ of annihilation energy that the nugget thermalizes from its accretion [19], thus $F_{tot} = (1-g)F_{ann}$. For atmospheric and surface densities encountered at Earth, the density-dependent effective temperature is expected to be [19]

$$T_\rho = 90\ \text{keV}\left[\left(\frac{1-g}{0.9}\right)\left(\frac{f}{0.067}\right)\left(\frac{u_n}{10^{-3}\ c}\right)\left(\frac{\rho}{\text{g cm}^{-3}}\right)\right]^{\frac{4}{17}} \qquad (3)$$

where f is related to the accretion efficiency of the AQN, u_n is the AQN velocity relative to Earth, and ρ is the density of the medium. The annihilation efficiency terms are somewhat uncertain; typical values given are $g \sim 0.1$ and $f \sim 0.067$ [19].

A firm upper bound on the maximum AQN temperature T_{max} comes from the requirement that the radiation pressure just outside the surface of the AQN should not exceed the level required to accelerate the accreting matter away from the path of the nugget. A previous qualitative analysis [23] of the effects of radiation pressure of incoming material in the Earth's atmosphere estimated that T would saturate at densities $\rho \sim 10^{-3}$ g cm^{-3} in the lower atmosphere, giving $T_{max} \sim 10$ keV. This estimate did not account for the likely photo-ionization of the region very near the nugget and thus probably underestimated T_{max} [25], since the radiation pressure primarily depends on the cross section for photon momentum transfer with incoming nuclei. Another possible accretion-limiting effect was also discussed in reference [23], that of momentum transfer to the incoming nuclei via scattering off positrons in the AQN electrosphere surrounding the nugget. We first discuss the radiation pressure bound, the return later to the effects of positron scattering.

To illustrate these effects, consider the case of a nugget with $B = 10^{24}$, and $T \sim 10$ keV ($\sim 10^8$ K) accreting material at sea-level Earth-atmospheric density $\rho \sim 10^{-3}$g cm^{-3} at a velocity of 200 km s^{-1}. For this case, the AQN luminosity is $L_{tot} = 4\pi R_n^2 F_{tot} = 2 \times 10^6$ W. The intensity just outside the surface of the nugget is $I_{surf} = F_{tot} \sim 1.6 \times 10^{19}$ W m^{-2}. Since a large fraction of this intensity is emitted as soft X-rays, for which the photo-ionization cross section on air will far exceed the momentum-transfer cross section σ_N, the incoming material will be fully ionized before it approaches the AQN surface. The residual momentum-transfer cross section on the stripped nuclei is not well-documented, but it cannot exceed the incoherent atomic scattering cross section at keV photon energies, thus we estimate $\sigma_N \lesssim 10^{-2}$ barn $= 10^{-30}$ m^2. The required acceleration to displace the nuclei from the oncoming nuggets path is of order $a_{min} = \Delta u/\Delta t \sim u_n^2/R_n$, and thus the radiation pressure is determined from

$$\frac{I_{surf}}{c} \leq \frac{m_N u_n^2}{\sigma_N R_n} \tag{4}$$

where $m_N \sim 2.2 \times 10^{-26}$ kg is the typical atomic mass, for nitrogen in this case. This yields, for the example above, $I_{surf} \lesssim 3 \times 10^{30}$ W m^{-2}, many orders of magnitude above the the AGN radiance in this case. Bounding the surface emissivity with this then bounds the AQN temperature:

$$\frac{16}{3} \frac{\sigma_{SB} T^4 \alpha^{5/2}}{\pi} \left[\frac{T}{m_e}\right]^{\frac{1}{4}} \lesssim \frac{m_N u_n^2 c}{\sigma_N R_n} \tag{5}$$

and since the AQN radius depends on the number of baryons B as $R_n \sim 10^{-7}(B/10^{24})^{1/3}$ m^2 [20]:

$$T_{max} \lesssim 4.5 \text{ MeV} \left[\left(\frac{u_n}{200 \text{ km s}^{-1}}\right)^2 \left(\frac{m_N}{14 \text{ amu}}\right) \times \left(\frac{\sigma_N}{10^{-30} \text{ m}^2}\right)^{-1} \left(\frac{B}{10^{24}}\right)^{-\frac{1}{3}}\right]^{\frac{4}{17}} . \tag{6}$$

Of course, at several MeV AQN surface temperatures, external nuclear interactions and associated energy release will become important, and the luminosity of the nugget will be so high that other limiting effects are likely to obtain well before these temperatures are reached.

Another potential limiting effect is that the ram pressure of the fraction of stripped nuclei that mechanically collide with positrons in the electrosphere of the nugget will form a bow shock to the propagating nugget, and this will limit the ingress of other matter. This constraint was discussed briefly by Lawson [23], where it was argued that once the kinetic temperature of the positrons approached that of the incoming nuclei, they would begin to scatter off the positrons and a negative feedback condition would obtain. However, the momentum transfer of the electrosphere to incoming nuclei is given by the Rutherford scattering cross section for positrons on the stripped nuclei. As the nugget temperature increases, the Rutherford scattering cross section decreases quadratically with the effective temperature $\sigma_R(T) \propto T^{-2}$. In contrast, the AQN electrosphere temperature increases only slowly with annihilation rate $T \propto F_{ann}^{4/17}$ [19], causing this process to decrease in efficiency in deflecting nuclei as the accretion process increases. Thus it appears that positron scattering cannot produce a negative feedback accretion-limiting condition.

A more likely source of negative feedback may come from backscattering at the quark-matter interface of the nugget; the accretion efficiency term f used above arises from this process [19], but it is unclear what the temperature dependence of this effect might be. An estimate of this process is beyond our scope, so in what follows we assume that AQN surface temperatures approaching 100 keV (a few percent of the radiation pressure T_{max} derived here) in solid materials are not excluded yet by any accretion constraints.

III. AQN INTERACTING AT EARTH

A. Lithosphere interactions

We first consider interactions of these AQN in Earth's lithosphere. The kinetic energy loss for either quark or antiquark nuggets was first derived in the analysis of de Rujula & Glashow [12]:

$$\frac{dE}{dx} = -A_n \rho(x) u_n^2 \tag{7}$$

where A_n is the cross sectional area of the nugget, and $\rho_(x)$ is the density along the track x. Setting $\rho(x)$ to the average density $\langle\rho\rangle$ along the track,

$$u_n(x) = u_n(0) e^{-A_n \langle\rho\rangle x/M_n} . \tag{8}$$

If an antiquark nugget stops in the Earth through loss of kinetic energy, it will then subsequently completely annihilate, and the energy deposition in that case will equal its remaining mass energy. For AQN to remain viable dark matter candidates, the total power contribution through this process to the Earth's thermal energy budget must not exceed that of known

sources. The current geothermal energy budget of the Earth is $P_{geo} \sim 44 \pm 3$ TW [28, 29], and of order half of this must be attributable to radionuclide decay; the remainder is still a subject for debate, although a major fraction must be residual heat from the gravitational collapse of formation. If we allow that of order $P_{geo}/4 \sim 11$ TW of the current geothermal energy budget could be available to external heating from AQN annihilation, then the rate of captured AQN must satisfy $dm/dt \leq P_{geo}/(4c^2) = 0.12$ grams/sec. At the current firm lower bound for AQN baryon number $B_{min} \sim 10^{20} = 0.16$ mg, a flux of AQN at this mass, equal to the dark matter density, is of order 10^6 s^{-1} over the whole Earth, thus the capture probability must not exceed about 10^{-3} per nugget. The required flux to match the DM falls as B^{-1}, and the mass-energy rises as B, so this constraint is constant with AQN mass. So far we have ignored the energy deposited during the transit of the nugget; we return to that below.

If we require that no more than 0.1% of all AQN lose enough kinetic energy via equation 7 to be captured by Earth, this translates into a requirement that the velocity attenuation in equation 8 above can only fall below the escape velocity in 0.1% of all AQN tracks. Taking $u_n(0) = 200$ km s^{-1}, and the Earth escape velocity $u_{esc} \sim 11$ km s^{-1}, we evolve an initial Maxwell-Boltzmann velocity distribution by assuming equation 8 above, with a mean travel distance of $\bar{x} = 4R_E/3$, the mean chord distance through the Earth for random tracks [26, 27]. By then requiring that the cumulative evolved Maxwellian have no more than 0.1% of its final velocities below u_{esc}, we find the following constraint if all of the dark matter consists of AQN of mass equal to or greater than B_{min}:

$$B_{min} \;=\; 2.6 \times 10^{24} \tag{9}$$

where we have used a mean density of $\langle \rho \rangle = 5500$ kg m^{-3} for the Earth, and a nugget area $A_n = \pi R_n^2$, with $R_n = 10^{-7}(B/10^{24})^{1/3}$ m. It thus appears that geothermal considerations rule out AQN of masses less than about 4 grams, well above prior constraints. This limit can only be evaded if the velocity distributions of the AQN are decidedly non-virial, but a similar constraint will obtain on whatever velocity distribution is present.

Now consider the emissivity in lithosphere transit of a flux of AQN well above B_{min} given here, with a nearly mono-mass spectrum with $B \sim 10^{25}$. As the nugget enters the solid crust at 200 km s^{-1}, the temperature rises to around 120 keV (using expected values for f, g above, and a mean density of 5.5 gm cm^{-3}, giving an initial luminosity $P_i = 4\pi\, R_n^2\, F_{tot} \sim 3.7 \times 10^{11}$ W. At this mass, the velocity attenuation length is $M/(A_n\langle\rho\rangle) \sim \pi R_E$, and using the mean chord of $4R_E/3$, the velocity at exit is $u_f \sim (2/3)u_n(0)$, so the mean velocity is of order $0.8u_n(0)$, and thus the average power is $0.8P_i \sim 3 \times 10^{11}$ W. The integrated rate of energy being continuously deposited, if the dark matter consists entirely of nuggets of this mass, is $P_{tot} \sim 48$ TW. This level of thermal energy also exceeds the current ~ 44 TW geothermal energy budget of the Earth[28, 29]. Using again the requirement that AQN contribute no more than 1/4 of the current geothermal energy, we may place a constraint on the maximum temperature at $B \sim 10^{25}$: in this case $T_{max} \leq 120$ keV$(11/48)^{4/17} = 85$ keV.

It might appear that the T^4 dependence of the AQN luminosity does not leave much headroom for larger nugget masses, since the accretion rate grows with the cross section of the nugget. Clearly, the radiation pressure constraint used in deriving equation 6 above is far less restrictive than the constraints from geothermal power. However, the temperature is to first order only dependent on the density of the medium, rather than nugget mass. Also, since the accretion cross section grows as $B^{2/3}$, and the flux required to match the dark matter density decreases as B^{-1}, higher masses are possible, but again will be marginally close to violation of the geothermal constraints, unless the maximum temperature or accretion efficiency is lower than initial estimates.

B. AQN meteors?

Meteor-like events originating from quark nuggets or *nuclearites*, as they are termed in this context, were first considered by de Rujula & Glashow [12]. Such events would have very rapid transits through the atmosphere due to their high velocities relative to solar system meteors; At $u_n \sim 200$ km s^{-1} they are a factor of 3 faster than the fastest meteors. These events are estimated to have visual magnitudes given by

$$V = 10.8 - 1.67\log_{10}(m/10^{-6}) + 5\log_{10}(h/10\text{ km}) \tag{10}$$

where m is the mass in grams, and h the distance from the observer. For $B \sim 10^{24}$ and a distance of around 30 km, this gives $V \sim 3$, easily detectable against the night sky, although not dramatic compared to many visual meteors. This signature was used by Porter *et al.* [31, 32] to set limits on the fraction of nuclearites possible as dark matter for a range of different discrete masses covering 10^{-4} to ~ 10 g, based on observations using cosmic-ray air Cherenkov telescopes.

For antiquark nuggets, the optical signature is not dramatically different than for quark nuggets, except at relatively low elevations. Propagating in the Earth's lower atmosphere at a temperature of 10 keV, an AQN with $B \sim 10^{24}$ produces megawatt total bolometric luminosity, as noted above. However, the AQN power restricted to the optical band is of order 1 kW, equivalent to relatively bright meteor with visual magnitude of $m_V \sim -1$ [30] observed at typical meteor distance of order 100 km. However, in contrast to a meteor which reaches its peak luminosity high in the atmosphere, an AQN would not achieve its peak temperature until near ground level. At the typical ~ 80 km altitude of a meteor, the AQN temperature would be a factor of 10 lower, and the luminosity more like 100 mW, orders of magnitude fainter than near the ground.

The observations of Porter *et al.* [31, 32] focused on distances of 20-30 km, and elevations of 15-20 km, where the AQN luminosity is closer to that of normal quark nuggets. The constraints from these experiments thus apply at least equally to both quark and antiquark nuggets, and lacking the necessary information about their analysis, we cannot say if the equivalent AQN constraints from their data would be more restrictive in detail.

C. Thermal radio signatures

While the visual emissivity of an AQN with $B \sim 10^{24}$ passing through the terrestrial atmosphere may be easily missed, the flat spectrum displayed in Fig. 1 produces a surprisingly strong broadband radio signature, of order 10 mW GHz^{-1} in the VHF to microwave band even at the lowest AQN temperature considered, and far more at the higher ones. The expected radio flux density in this spectral region for an AQN transiting the atmosphere is thus of order [23]

$$S_{AQN} \sim 8 \times 10^{-23}\ \mathrm{W\ m^{-2}\ Hz^{-1}} \left(\frac{T(\rho)}{10\ \mathrm{keV}}\right)^{13/4} \left(\frac{\langle D\rangle}{100\ \mathrm{km}}\right)^{-2} \left(\frac{B}{10^{24}}\right)^{2/3} \quad (11)$$

where $T(\rho)$ is given by equation 3 above, and we have ignored the weak logarithmic dependence. For an AQN transiting a solid material, viewed from outside the material, there are additional terms due to the attenuation of radio signals in the solid material, and the Fresnel transmission coefficient $\mathcal{F}_T$ for the emission as it passes through the interface. Thus

$$S_{AQN,solid} = S_{AQN}\ \mathcal{F}_T\ e^{-2d/L_{atten}} \quad (12)$$

where d is the pathlength of the radio emission in the solid, and L_{atten} is the field attenuation length in the medium.

Receiver thermal noise levels at a typical receiver system temperature of $T_{sys} \lesssim 300$K, by comparison, are typically $P_n = kT_{sys}\Delta f \lesssim 5$ pW in a GHz of bandwidth. The broadband AQN radio flux density is thus likely to be well above thermal noise for large distances from the track. This will of course depend on the mean distance $\langle D\rangle$ from the track, as well as the time τ over which the AQN track remains in the primary field-of-view, or half-power beamwidth H, of a given antenna. This in turn depends on the antenna gain (or directivity) G. For moderately directive antennas of a few dBi of gain or more, $G \sim 27000(H^\circ)^{-2}$ where the beamwidth H is given in degrees here, and thus for $u_n \sim 200$ km s^{-1}, $G \sim 10$, and $\langle D\rangle \sim 100$ km, the in-beam residence time is 0.3-0.5 seconds; however, receiver gain instabilities make it practical to limit the integration time $\tau \lesssim 0.1$ seconds, giving several samples per transit per beam. An antenna of constant gain G over a passband from f_1 to f_2 has an average effective area (for a flat spectrum source) of $A_{eff} = 2Gc^2/(4\pi f_1 f_2)$ and the minimum detectable signal power of this antenna with receiver bandwidth $\Delta f = f_2 - f_1$ and integration time τ is

$$\sigma_s = \frac{kT_{sys}}{A_{eff}\sqrt{\Delta f \tau}}\ . \quad (13)$$

Assuming the integration time τ is matched to the expected beam crossing time for $u_n \sim 200$ km s^{-1}, the limiting sensitivity is

$$\sigma_s \simeq 10^{-24}\ \mathrm{W\ m^{-2}\ Hz^{-1}} \left(\frac{T_{sys}}{300\ \mathrm{K}}\right)\left(\frac{\sqrt{f_1 f_2}}{490\ \mathrm{MHz}}\right)^2 \times \left(\frac{\Delta f}{1\ \mathrm{GHz}}\right)^{-1/2}\left(\frac{G}{10}\right)^{-3/4}\left(\frac{\langle D\rangle}{100\ \mathrm{km}}\right)^{-1/2}\ . \quad (14)$$

Comparing this to equations 11 and 12 indicates that such events are detectable with a modest antenna collecting area and receiver out to distances of several hundred km, even at the lowest AQN temperature considered here. The advantage in detection of thermal radio emission as compared to other possible forms of beamed emission, such as geosynchrotron emission considered in reference [23], is that the acceptance solid angle does not require observation very close to the axis of the AQN velocity. Thus for an isotropic flux of AQN, thermal radio detection will have a far greater probability.

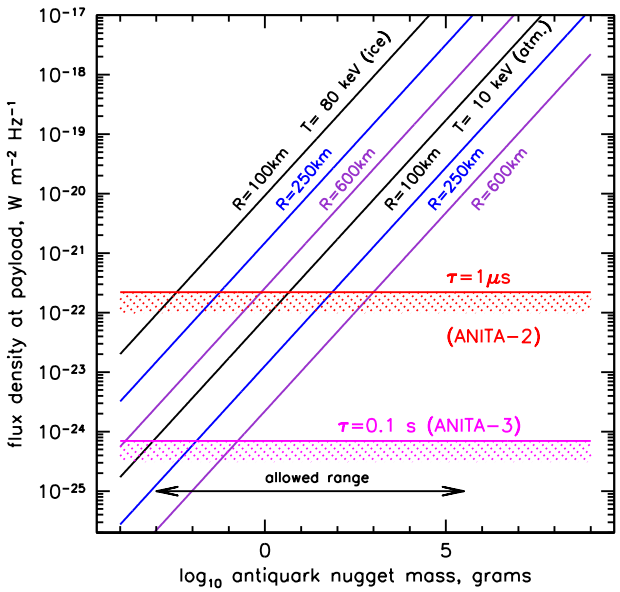

FIG. 2: *Estimated flux density and sensitivity for ANITA for two different AQN temperatures and three different distances, for AQN transiting in atmosphere ($T = 10$ keV), or Antarctic ice ($T = 80$ keV), with typical estimated attenuation losses and Fresnel coefficient. The thermal noise levels for two different integration times are shown.*

IV. THERMAL RADIO DETECTION PROSPECTS

Given that the distance scale for detection is plausibly hundreds of kilometers even at the lowest AQN temperatures, and perhaps much more at higher temperatures, it is evident that a ground-based detector is at a disadvantage compared to the synoptic field-of-regard of suborbital or orbital platforms. Since the AQN luminosity appears to rise by orders of magnitude once it enters solid material, and since terrestrial ice in the Earth's cryosphere is highly transparent in the VHF and

UHF radio range [33, 34], suborbital/orbital observations of Antarctic or Arctic ice sheets afford perhaps the most sensitive possible channel for AQN detection. We thus conclude by estimating to first-order the sensitivity of this approach, using the parameters of the Antarctic Impulsive Transient Antenna (ANITA) suborbital payload [35], which has completed two flights (ANITA-1: 2006-2007; ANITA-2: 2009-2010) and is scheduled to complete a third next year. ANITA has enough directional capability to establish the velocity of an AQN candidate, a crucial discriminator against other possible background events such as meteors.

For a radio detector viewing Antarctica synoptically from stratospheric altitudes, as in the case of ANITA, the horizon is at a distance of $600-700$ km, and the area viewed is over 1M km^2 out to the horizon. To illustrate the range of sensitivity, Fig. 2 plots the AQN signal and thermal noise levels based on equations 11, 12, & 14 above, using instrument parameters for ANITA-2 and ANITA-3 [36], for a range of AQN masses that are currently unconstrained, for several different distances. For ANITA-2, the $\tau = 1$ μs integration time arose in the ambient radio-frequency (RF) power monitoring system, an auxiliary detector to the primary 2.6 Gsample/sec waveform recorder which captures only a 100 ns time window. The ambient RF power monitor samples each antenna signal at about 8 Hz, but with a much shorter integration time due to analog-to-digital conversion related constraints. However, these samples occur for both polarizations, and there are 2-3 antennas sampling each azimuthal direction at 22.5° azimuth intervals. Since the thermal AQN signals are unpolarized, the two ANITA polarization samples are independent, as are the 2-3 different antennas per azimuthal sector, and thus an AQN signature can be detected with high-confidence by requiring the signals to appear in a majority coincidence of all of these independent channels. For ANITA-3 the design will allow for much longer integration times per RF power monitoring signal, and thus the sensitivity will be substantially improved.

It is evident from Fig. 2 that AQNs transiting either the atmosphere or ice sheets can be detected, but to ensure that these are distinguished from the many forms of anthropogenic and other radio-frequency interference, the AQN track needs to be detected over an azimuth range such that a velocity can be unambiguously determined. This requires a projected azimuthal span for the track of order $\Delta\phi \gtrsim 20^\circ$ for ANITA [35], so that at least two adjacent azimuthal sectors show a signal; this is possible over this range of azimuth since the ANITA antenna beams overlap each other in adjacent azimuthal sectors.

To estimate the limiting sensitivity for ANITA, we must integrate over the acceptance area, solid angle, and detection efficiency. The number of detected events N as a function of the baryon number B of the AQN can be written

$$\frac{dN}{dB} = T_{obs}\int_0^{4\pi} d\Omega \int_0^{R_H} 2\pi r dr \mathcal{F}(B)\mathcal{E}(B,r,\theta,\phi,\rho) \quad (15)$$

where T_{obs} is the integrated observation time, R_H is the distance to the horizon, $\mathcal{F}(B)$ is the flux of AQN, and $\mathcal{E}(B,r,\theta,\phi,\rho)$ is the instrumental detection efficiency (bounded between [0,1]) as a function of baryon number, distance r, angular track directions θ,ϕ, and medium density ρ.

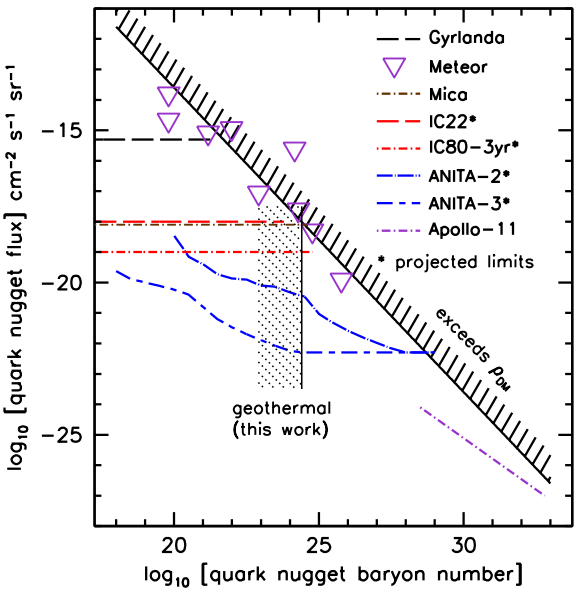

FIG. 3: *Existing and projected limits on quark and antiquark nugget fluxes with respect to dark matter density (diagonal hatched curve). The geothermal limits and ANITA projections are for AQN, from the present work. All other constraints apply to both quark nuggets and AQN.*

The requirement on azimuth span above constrains the track to be relatively horizontal, such that at distance D from the payload, the zenith angle range is limited by $\Delta\theta \sim (10\text{ km})/(D sin\Delta\phi)$ for events in the atmosphere, $\Delta\theta \sim (2.0\text{ km})/(D sin\Delta\phi)$ for in-ice tracks. Using these constraints, and requiring that the signal-to-ratios $S_{AQN,atmos}/\sigma_s \geq 3$ or $S_{AQN,ice}/\sigma_s \geq 3$ for a trigger, we have simulated the detection of AQNs with ANITA to determine the limiting sensitivity using Monte Carlo methods.

The results are shown in Fig. 3 where we have shown the curves based on the flown ANITA-2, and planned ANITA-3 instruments. For ANITA-2, this applies to data that has been already acquired, but has not yet been analyzed for this type of signal; here we assume that no background events are found. For ANITA-3 we use projected performance estimates provided by the ANITA collaboration, and a 30 day livetime is assumed, similar to what was achieved for ANITA-2. The inflection in the sensitivity curve in each case is due to the crossover of the effects of ice detection, which is more efficient at lower AQN masses, and atmospheric detection, which has a larger available solid angle and is more effective at higher AQN masses. For both ANITA-2 and ANITA-3, the sensitivity eventually saturates the available area for very high AQN masses, and the curves flatten out.

We have also included in Fig. 3 the constraint from geothermal power derived in this work; this limit is specific to antiquark nuggets rather than quark nuggets because it relies on the deposit of annihilation energy of the AQN. We plot for completeness several other actual (rather than projected) lim-

its on quark nuggets: from the Lake Baikal detector [24], from the mica track analysis [15], the optical limits from analysis of meteor-like events [31, 32], and from analysis of the Lunar seismic noise detected in the Apollo 11 mission [14]. It is evident that quark nuggets of either normal or antiquark matter are now strongly constrained below baryon number $B \sim 10^{24}$ where they can no longer comprise more than a few percent of the dark matter.

For the IceCube curves in Fig. 3, both are still projections, although the data for IceCube 22 already exists. For IceCube 80, the projection is for three years of data, which will be achieved in early 2014 [37]. Analysis of existing ANITA-2 data for these event signatures has begun, and results may be expected within the next year. Thus it appears that this very interesting region of parameter space for quark nugget dark matter is within reach of several current experiments, and we can hope for either detections or compelling limits in the near future.

V. CONCLUSIONS

We have considered the observable consequences of a proposed scenario in which primordial antiquark nuggets comprise a significant fraction of the dark matter. We analyze the thermal behavior and emission of AQN as they enter the terrestrial atmosphere, lithosphere, and cryosphere, and accrete matter accordingly in each locale. We find that neither radiation pressure from the AQN, nor Rutherford scattering of incoming matter off the positron electrosphere of the AQN are effective at limiting the accretion, at least until AQN temperatures approach several MeV. Adapting prior analysis, we find temperatures of order 100 keV are possible for AQN transiting solids such as rock and ice.

AQN transiting the lithosphere will behave differently than quark nuggets, since if they are captured by the Earth through their loss of kinetic energy during transit, they will eventually completely annihilate in the Earth's crust. Considerations of such capture and annihilation lead to a new geothermal limit on the flux of AQN which constrains them to be below the dark matter density for baryon number $B \lesssim 3 \times 10^{24}$, a new constraint specific to AQN.

By considering the thermal radio emission of accreting AQN in the cryosphere and atmosphere, in the baryon number range $B = 10^{20-28}$, we find that such emission should be well within the sensitive range of a synoptic balloon-borne instrument such as ANITA. We estimate that data already in hand should be capable of constraining the flux of AQN over a mass range that is otherwise not currently constrained, and that the planned ANITA-3 flight could improve these constraints by several orders of magnitude.

We thank both NASA and the US Department of Energy, High Energy Physics Division for their generous support of this work, and Kyle Lawson for very useful input. We also thank the ANITA collaboration for providing information regarding ANITA-3 performance, especially Gary Varner and Patrick Allison for their help in understanding the existing instrument performance.

[1] M. Bartlemann, Rev. Mod. Phys. 82, 331382 (2010).
[2] Salucci, P.; Nesti, F.; Gentile, G.; Martins, C. F 2010 A&A 523.
[3] S. Garbari, C. Liu, J. I. Read, G. Lake MNRAS, in press, 2012.
[4] The actual value of the local dark matter density remains a topic of lively debate, with some estimates as low as zero, to values about two to three times that quoted here.
[5] D. T. Cumberbatch, G. D. Starkmann, J. Silk, PRD 77,063522.
[6] A. H. G. Peter, M. Rocha, J. S. Bullock, M. Kaplinghat, arXiv:1208.3026, (2012).
[7] E. Witten, Phys. Rev. D 30, 272 (1984).
[8] Strange quark matter in the form of a stable star in hydrostatic equilibrium was first discussed by N. Itoh, Prog. Theor. Phys., 44, 291-292 (1970)
[9] Wilczek et al., Phys. Lett. B 422, 247, 1998
[10] G. Lugones, J. E. Horvath, Phys.Rev. D69 (2004) 063509.
[11] F. Weber, Prog. Part. Nucl. Phys. 54, 193 (2005).
[12] A. de Rujula and S. Glashow, Nature (London) 312, 734 (1984).
[13] D. Anderson, E. Herrin, V. Teplitz, and I. Tibuleac, Bull. Seismol. Soc. Am. 93, 2363 (2003).
[14] E. T. Herrin, D. C. Rosenbaum, V. L. Teplitz, PRD 73, 043511 (2006).
[15] P. B. Price, *et. al*, Phys. Rev. Lett. 52, 1265, (1984).
[16] Neil D. Selby, J. B. Young, and Alan Douglas Bull. Seismol. Soc. America December 2004 94:2414-2415.
[17] J. Madsen and K. Riisager, Phys. Lett. 158B, 208 (1985).
[18] J. Madsen, Lect. Notes Phys. 516 (1999) 162-203.
[19] M. M. Forbes, and A. R. Zhitnitsky, PRD 78, 083505, (2008).
[20] M. M. Forbes, K. Lawson, and A. R. Zhitnitsky, PRD 82, 083510, (2010).
[21] K. Lawson, PRD 83, 103520, (2011).
[22] K. S. Cheng and T. Harko, Ap. J. 596, 451, (2003).
[23] K. Lawson, arXiv:1208.0042 (2012).
[24] A. R. Zhitnitsky, JCAP 10, 010, (2003).
[25] K. Lawson, personal communication.
[26] D. Berengut, Office of Naval Res. Tech. Rep. 191, Dept. of Statistics, Stanford Univ. (1971).
[27] W.J.M. de Kruijf, J.L. Kloosterman, Ann. of Nucl. Energy 30 (2003) 549553.
[28] J. H. Davies and D. R. Davies, Solid Earth, 1, 524, 2010.
[29] Jaupart, C., Labrosse, S., and Mareschal, J.-C., Treatise on Geophysics, Vol. 7, Mantle Convection, edited by: Bercovici, D., Elsevier, 253303, 2007
[30] E. Opik, Irish Astron. Journ. 3, 165, 1955.
[31] N. A. Porter, D. J. Fegan, G. C. MacNeill, & T. C. Weekes, Nature 316, 49 (1985); doi:10.1038/316049a0
[32] Porter, N. A., Cawley, M. F., Fegan, D. J., MacNeill, G. C., & Weekes, T. C., Irish Astronomical Journal (ISSN 0021-1052), vol. 18, March 1988, p. 193-196.
[33] S. Barwick, D. Besson, P. Gorham, D. Saltzberg, J. Glaciol. 51, 231 (2005).
[34] D. Besson, R. Keast and R. Velasco, Astropar. Phys. 31, (2009) 348.
[35] P.W. Gorham et al. [The ANITA Collaboration], Astropart. Physics 32, 10-41, (2009).
[36] G. Varner and P. Allison, personal communication.
[37] B. Christy *et. al* [IceCube Collaboration], 30th ICRC, (2007).